The Astrophysical Journal Supplement Series, 191:96–112, 2010 November doi:10.1088/0067-0049/191/1/96

INFRARED SPECTRA AND OPTICAL CONSTANTS OF NITRILE ICES RELEVANT TO TITAN'S ATMOSPHERE

Marla H. Moore[1], Robert F. Ferrante[2], W. James Moore[3], and Reggie Hudson[1]
[1] NASA Goddard Space Flight Center, Code 691, Greenbelt, MD 20771, USA; Marla.h.moore@nasa.gov
[2] Chemistry Department, US Naval Academy, 572 Holloway Road, Annapolis, MD 21402, USA
[3] USRA NASA Goddard Space Flight Center, Code 691, Greenbelt, MD 20771, USA
Received 2010 March 12; accepted 2010 September 13; published 2010 October 25

ABSTRACT

Spectra and optical constants of nitrile ices known or suspected to be in Titan's atmosphere are presented from 2.0 to 333.3 μm (~5000–30 cm^{-1}). These results are relevant to the ongoing modeling of *Cassini* CIRS observations of Titan's winter pole. Ices studied are: HCN, hydrogen cyanide; C_2N_2, cyanogen; CH_3CN, acetonitrile; C_2H_5CN, propionitrile; and HC_3N, cyanoacetylene. For each of these molecules, we also report new cryogenic measurements of the real refractive index, n, determined in both the amorphous and crystalline phases at 670 nm. These new values have been incorporated into our optical constant calculations. Spectra were measured and optical constants were calculated for each nitrile at a variety of temperatures, including, but not limited to, 20, 35, 50, 75, 95, and 110 K, in both the amorphous phase and the crystalline phase. This laboratory effort used a dedicated FTIR spectrometer to record transmission spectra of thin-film ice samples. Laser interference was used to measure film thickness during condensation onto a transparent cold window attached to the tail section of a closed-cycle helium cryostat. Optical constants, real (n) and imaginary (k) refractive indices, were determined using Kramers–Kronig analysis. Our calculation reproduces the complete spectrum, including all interference effects.

Key words: catalogs – infrared: planetary systems – methods: laboratory – planets and satellites: individual (Titan) – techniques: spectroscopic

Online-only material: machine-readable tables

1. INTRODUCTION

Analysis of *Voyager* Infrared Interferometer Spectrometer and *Cassini* Composite Infrared Spectrometer data of Titan in the 8–500 μm region reveals signatures of a complex array of atmospheric organic gas-phase molecules (e.g., HCN, C_2N_2, HC_3N, CH_3CN, CH_4, C_2H_6, and C_3H_4; see Table 1). In addition, strong evidence for ice features due to HCN, HC_3N, and C_4N_2 exists. For example, in Titan's atmosphere the lattice band of HCN at 166 cm^{-1} has been identified in spectra taken of the winter pole (Samuelson et al. 1997), the ν_6 band of HC_3N ice at 504 cm^{-1} has been positively identified (Anderson et al. 2010), and the ν_8 band of dicyanoacetylene (C_4N_2) ice at 478 cm^{-1} has been positively identified (Khanna et al. 1987) and quantitatively fit (Samuelson et al. 1997). These interpretations of Titan observations depend on knowledge of the spectra of various molecular solids suspected to be present. The physical state (crystallographic phase) and temperature are important factors in molecular identifications since they can cause large frequency shifts in an ice's spectral features and band splittings that change the shape, intensity, and width of an absorption. Accurate optical constants of molecular solids for different physical states and temperatures are extremely useful for fitting emission features using rigorous radiative transfer calculations and models of optical effects of condensate particle sizes and distributions.

Previous laboratory studies of several crystalline nitrile ices relevant to the atmosphere of Titan, including the extraction of optical constants from measured spectra, were published in a series of papers from the University of Maryland between 1988 and 1996. Ospina et al. (1988) showed plots of calculated n and k values for crystalline phase C_2N_2 from 4000 to 200 cm^{-1}, where n and k are the real and imaginary parts of the complex index of refraction. Following this, 4000–450 cm^{-1} spectra and optical constants of HCN and HC_3N were tabulated and published by Masterson & Khanna (1990). Dello Russo & Khanna (1996) published results on crystalline HCN, C_2N_2, HC_3N, C_2H_5CN, and CH_3CN at 35 and 95 K, including mid- and far-infrared spectra at 35 K and tables of n and k values from 5000 to 80 cm^{-1}.

In this paper, we provide for the first time measurements of condensed HCN, C_2N_2, CH_3CN, C_2H_5CN, and HC_3N that include both amorphous and crystalline-phase ices from ~ 5000 to 30 cm^{-1} at a variety of temperatures. We have measured the real part of the index of refraction for these nitriles in both the amorphous and the crystalline phase at 670 nm (14900 cm^{-1}), and have included these values in the calculations of the optical constants. Older optical constant data that are available for these nitriles have not included measured values for the visible index of refraction. Overall the goal of the present work is to provide a database of optical constants that can be used by the astronomical community, similar to the H_2O ice work of Hudgins et al. (1993). A digital version of our data and optical constants is available at the Astrophysical Journal Web site and the Cosmic Ice Laboratory's Web site[4].

2. LABORATORY PROCEDURES

Figure 1 is a schematic of the ice sample holder and vacuum chamber used in these studies. Infrared absorption spectra were recorded with a Perkin Elmer Spectrum GX single-beam spectrometer capable of measurements from 7800 to 30 cm^{-1} (1.28–333 μm). Wavenumber positions are accurate

[4] http://science.gsfc.nasa.gov/691/cosmicice

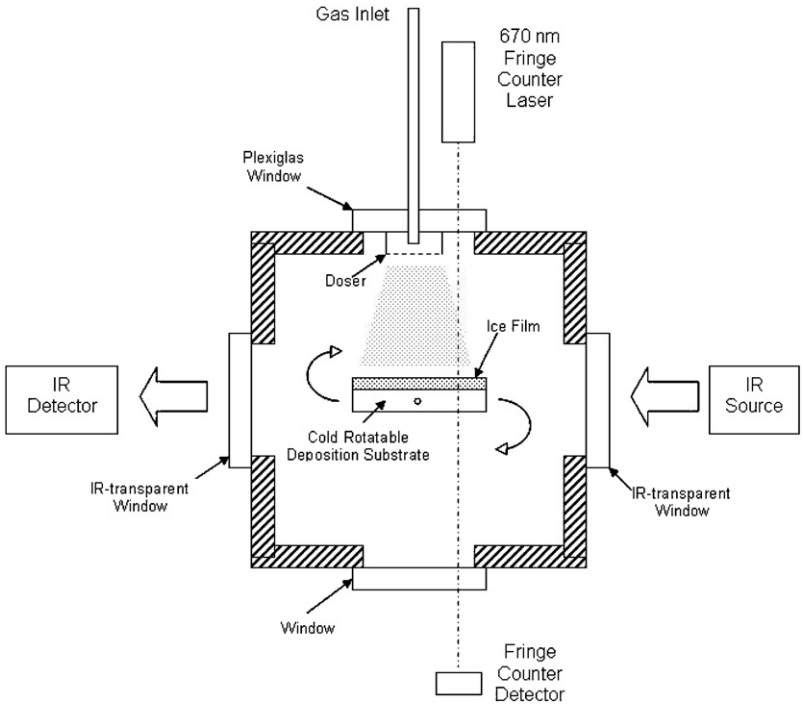

Figure 1. Schematic of experimental setup. The sample chamber has two infrared-transparent windows and an appropriate substrate onto which the ice film is formed. Infrared spectra are measured when the substrate is rotated 90° clockwise from the position shown.

Table 1
Molecules in Titan's Atmosphere

Molecule	Phase in Titan's Atmosphere (p = proposed)	Condensation Temp. (K)[a]	Temp. of Phase Change (K)[b]
Nitriles			
Hydrogen cyanide, HCN	Gas[c], solid (p)[a]	125	120
Cyanogen, C_2N_2	Gas[d]	100	90
Cyanoacetylene, HC_3N	Gas[d], solid (p)[a,e]	120	110
Dicyanoacetylene, C_4N_2	Solid[f]	112	...
Acetonitrile, CH_3CN	Gas[g]	100	130
Propionitrile, C_2H_5CN	Solid (p)[a,h]	81	140
Hydrocarbons			
Methane, CH_4	Gas[c]	72	20*
Ethane, C_2H_6	Gas[c], solid (p)[a]	72	65
Propane, C_3H_8	Gas[i]	81	75
Ethylene, C_2H_4	Gas[c]	...**	50
Acetylene, C_2H_2	Gas[c], solid (p)[a,e]	81	80
Methylacetylene, C_3H_4	Gas[i]	81	...
Diacetylene, C_4H_2	Gas[d]	117	...
Other			
Water, H_2O	Solid (p)[a]	120	130

Notes. [a] Coustenis et al. 1999, [b] Data on amorphous-to-crystalline phase changes from our laboratory, [c] Hanel et al. 1981, [d] Kunde et al. 1981, [e] Khanna 2005b, [f] Samuelson et al. 1997, [g] Bézard et al. 1993, [h] Khanna 2005a, [i] Maguire et al. 1981, * Crystalline transition (phases I and II), ** does not condense in Titan's atmosphere (Coustenis et al. 1999).

to 0.01 cm^{-1}. For mid-infrared experiments (7800–380 cm^{-1}), ices were grown on a KRS-5 or CsI substrate cooled by a closed-cycle helium refrigerator ($T_{min} \sim 16$ K) mounted in a high vacuum chamber ($P \sim 2 \times 10^{-7}$ torr when cold). The vacuum windows were KBr. For far-infrared experiments (700–30 cm^{-1}), ices were formed on a high-density polyethylene (HDPE) substrate. In this wavelength region the vacuum windows also were HDPE. Mid-infrared spectra were usually measured at a 2 cm^{-1} resolution using a mid-DTGS detector and a KBr beam splitter whereas far-infrared spectra had a 4 cm^{-1} resolution and were measured using a far-DTGS detector and a grid beam splitter. Scan accumulations varied from 100 to 256 in both spectral regions. In both the mid- and far-infrared regions, we accumulated four data points per resolution element.

In general, we used a uniform procedure for the collection of spectral data. First, the substrate window was cooled to 50 K (20 K for C_2N_2) and a background spectrum was recorded after rotating the window to face the infrared beam. The window next was rotated to face the gas inlet for the deposition of HCN, C_2N_2, CH_3CN, C_2H_5CN, or HC_3N. In each case an amorphous sample was produced. During deposition, the number of laser interference fringe maxima (m) recorded was used to calculate

Table 2
Measured Index of Refraction of Amorphous and Deposited Crystalline Phase Nitrile Ices at 670 nm

Molecule	Amorphous Phase		Deposited Crystalline Phase		Literature Values
	Deposit Temperature (K)	*n*-value	Deposit Temperature (K)	*n*-value	
HCN	30	1.30	120	1.39	1.2614 liquid[a] 1.36 solid[b]
C_2N_2	30	1.30	90	1.42	1.37[c]
CH_3CN	30	1.31	130	1.45	1.34 liquid[d]
C_2H_5CN	30	1.26	140	1.49	1.35[e]
HC_3N	30	1.41	110	1.43	1.39 liquid[f] 1.52 solid[g]

Notes. [a] Weast 1986, [b] Calculated by Masterson & Khanna 1990, [c] Assumed by Ospina et al. 1988, [d] Iloukhani & Almasi 2009; Riddick et al. 1986, [e] Assumed by Dello Russo 1994, [f] Moureu & Bongrad 1920, [g] Calculated by Khanna 2005b.

the ice's thickness using the equation

$$d = m\lambda/(2\sqrt{n^2 - \sin^2\theta}), \quad (1)$$

where d is the ice thickness (μm), λ is the laser's wavelength (0.670 μm), n is the index of refraction of the ice at λ, and θ is the angle between the incoming laser beam and the normal to the ice surface. Typically sin θ had a value <0.17. The laser fringes were weak when the HDPE substrate was used for far-infrared spectra, but in most cases could be distinguished. Using Equation (1), far-infrared film thicknesses were calculated to be from 1.5 to 6.3 μm. The estimated error in these thicknesses is ±3% since we know the maximum error in calculating the index of refraction is ±1.5% and the number of deposit fringes is accurate to $\frac{1}{4}$ fringe. This ±3% error in the thickness has an influence on the calculated extinction coefficient. As an example, we determined that the percentage change in the integrated extinction coefficient from 300 to 100 cm^{-1} for HCN is nearly equal to the percentage change in the thickness. For mid-infrared films, laser fringes were much stronger and Equation (1) could be used to calculate the initial ice thickness, but the final thickness determination was made by comparing the spectrum's channel fringes with a theoretical fringe set as described in Section 3.

After the amorphous ice was formed, it was warmed to 75, 95, and 110 K, and sometimes higher, stopping at the appropriate annealing temperature where the ice converted to a crystalline phase. Following the work of Dello Russo & Khanna (1996), the annealing temperatures were 120, 90, 130, 140, and 110 K for HCN, C_2N_2, CH_3CN, C_2H_5CN, and HC_3N, respectively. Ices were held at the annealing temperatures until spectral band shapes and peaks evolved to a final state that was not changed with increased annealing time. In all but one case, increased time at the annealing temperature led to noticeable sublimation. After annealing the ice is commonly referred to as "crystalline," and is the term we use throughout this manuscript. The quality of the crystalline structure may be slightly different using other formation techniques. For example, in some cases small spectral differences were found between the crystalline ice (formed by warming amorphous ice to the annealing temperature) and directly deposited ice (formed by quenching of gas at the annealing temperature). See Section 4.6 and the Discussion (Section 6) for more details.

After annealing, the ice was cooled to temperatures at or near 110, 95, 75, 50, 35, and 20 K. Specific selected temperatures varied slightly in a few cases; for 95 K, measurements ranged to 90 K, for 75 K, measurements ranged from 70 to 77 K, for 50 K they ranged to 55 K, and for 20 K they ranged to 14 K. Sample spectra at each temperature were ratioed against the initial background spectrum to give transmission spectra. Optical constants were calculated for both amorphous and crystalline ices as discussed in the next section.

Discussions of approaches for the direct experimental determination of the real part of the refractive index of condensed ice films are found in the literature (Tempelmeyer & Mills 1968; Seiber et al. 1971; Berland et al. 1995; Harrick 1971; Sill et al. 1980; Wood & Roux 1982; Westley et al. 1998; Satorre et al. 2008; Romanescu et al. 2010). For our measurements we used a separate, dedicated cryostat, similar in design to the one shown in Figure 1. During condensation of each nitrile, we simultaneously monitored interference fringes from two transmission–reflection–transmission (670 nm, 14900 cm^{-1}) solid-state laser beams at two angles of incidence ($\theta_1 = 6.^{\circ}758$ and $\theta_2 = 44.^{\circ}04$) to the cold substrate. The ratio t_1/t_2 of the lasers' periods of oscillation was used to calculate the refractive index using the well-known formula (e.g., see Satorre et al. 2008 or Romanescu et al. 2010):

$$n = (\sin^2\theta_2 - (t_1/t_2)^2 \sin^2\theta_1)^{1/2}/(1 - (t_1/t_2)^2)^{1/2}. \quad (2)$$

For index of refraction measurements, amorphous-phase nitriles were formed at 30 K, the lowest temperature of the substrate. Then, in a separate experiment, a crystalline-phase ice was made at the annealing temperature for that same nitrile. Table 2 presents a summary of our results. Calculated errors are of the order of 0.02. The sources of error are in the measurement of the two angles and the two time periods over which the sample's fringes are recorded. We used a standard method for the propagation of errors to estimate the uncertainties (Garland et al. 2002, p. 53). For comparison, we show previously measured values for these nitriles and values assumed by Dello Russo & Khanna (1996) or Ospina et al. (1988).

The nitrile gases used in these experiments were from a variety of sources. A small quantity of hydrogen cyanide (HCN) was synthesized in our laboratory (Gerakines et al. 2004). The gas released during the synthesis contained mainly HCN and CO_2 and was collected in a bulb cooled to 77 K. The CO_2 was removed by pumping when the bulb was immersed in an acetone slush bath at 178 K. Cyanogen gas (C_2N_2) was commercially available from Matheson (purity unknown). It was used without further purification although it contained a trace amount of CO_2.

Acetonitrile (99%) and propionitrile (99%) were purchased as liquids from Aldrich and were used without further purification. Each had a sufficient vapor pressure at room temperature to allow vapor condensation of the nitrile. Cyanoacetylene (HC_3N) was a gift from L. Stief (NASA Goddard) and H. Okabe (Catholic University of America). Its synthesis is described in Dello Russo & Khanna (1996).

3. OPTICAL CONSTANTS

As stated above, transmission spectra of nitrile ice films were recorded in the mid-infrared ($\sim$ 6000–400 cm^{-1}) and far-infrared ($\sim$ 600–30 cm^{-1}) regions. Spectra were then analyzed to extract each ice's real, n, and imaginary, k, refractive indices, similar to the work of Hudgins et al. (1993). Measurements in each spectral region required the use of a specific combination of beam splitter, substrate, and infrared-transparent windows. Switching from the mid- to the far-infrared regions and vice versa involved bringing the sample chamber (Figure 1) up to atmospheric pressure. This, in turn, meant that two separately prepared ices were needed to cover the full 6000–30 cm^{-1} range.

For each nitrile ice studied, the transmission of the sample–substrate combination was ratioed against the blank substrate's transmission in order to remove instrumental characteristics. The resulting spectrum, designated the measured spectrum, was more complicated than a flat line at transmission = 1 with superimposed absorption features from the sample. The spectrum usually suffered from losses due to scattering by an imperfect ice; it also exhibited effects of reflection at the vacuum–ice, ice–substrate, and substrate–vacuum interfaces. The first two of these reflections produce interference fringes, sometimes called channel spectra, a sinusoidal variation along the transmission spectrum's 100% line. Our spectral calculations (Goldstein 1989) readily modeled reflection, absorption, and interference effects. Minor modifications (Berning 1963) allowed us to calculate the relevant properties of the substrate without calculating interference effects within it. This approach applies to our laboratory substrates that have nonparallel surfaces. Consequently, as described below, we modified each measured spectrum to remove scattering effects and to correct incompletely formed channel fringes. Then we did a full modeling calculation of the ice's transmission spectra, including interference effects within the ice film.

One aspect of our measured spectra was an apparent transmission exceeding 1 (e.g., see Figure 2). This was a consequence of the ice acting, at some spectral frequencies, as an anti-reflection coating on the substrate. Consequently, in some cases, the transmission of the ice film-on-substrate was greater at some frequencies than the transmission of the substrate alone. Our calculations modeled this phenomenon.

Extraction of useful extinction coefficient data from our spectra required knowledge of the ice sample's thickness. Thickness measurements were done in several ways. (1) Counting interference fringes in the transmission of 670 nm laser light during growth of the ice and then calculating the thickness using Equation (1) (applied to far-infrared data). (2) Matching the calculated and observed channel fringes, similar to the method of Masterson & Khanna (1990) (applied to mid-infrared data). (3) If the material studied had absorption features in the region of spectral overlap of the mid- and far-infrared regions, we matched the product of the far-infrared extinction coefficient peak height and width at half-maximum to the mid-infrared value to indirectly determine the far-infrared ice thickness. (4) Recalculating the ice thickness after annealing. This was necessary because the process of annealing can cause compaction and possibly some sublimation of the ice film. In the mid-infrared we fit the channel spectrum of the annealed ice to obtain a new thickness. The observed fractional change in thickness between the pre- and post-annealed mid-infrared ices was applied to the sample's far-infrared data.

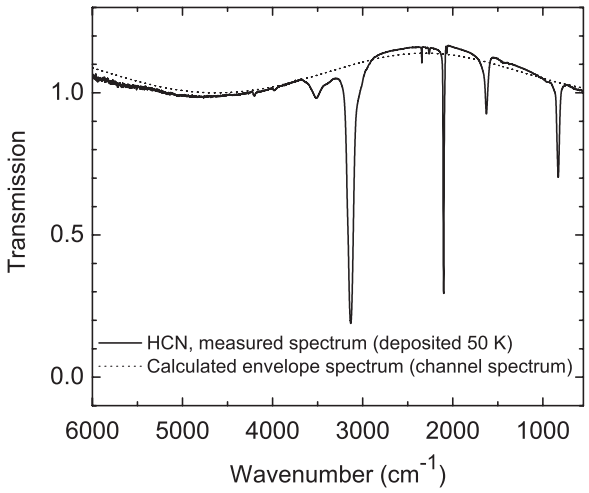

Figure 2. Measured transmission spectrum of HCN in the mid-infrared at 50 K shows well-developed channel interference fringes. A calculated channel (envelope) spectrum, using known ice thickness and index of refraction, is compared with the measured spectrum.

Measured spectra were corrected for losses due to scattering and amplitude departures from fully formed channel spectra, a result of ice flatness variations, by first creating a 100% line for the measured transmission spectrum that removed the scattering losses. In practice, we did this by converting from transmission (T) to absorbance ($A \equiv -\log_{10}(T)$), straightening the spectral trace to remove the channel fringes, adding/subtracting a vertical offset to get the baseline to zero, and then converting back to transmission. The resulting transmission spectrum will be referred to as the baselined spectrum in this paper.

We next calculated the expected transmission of a hypothetical ice with no absorptions, but having the same thickness and real refractive index as the ice under study and on the same substrate used for the experiment; we designate the result as the envelope spectrum. This calculation required knowledge of the ice's refractive index, n, which was determined at 670 nm in a separate experiment. Some reduction in the value of the index is expected when extrapolating to longer wavelengths. For example, the work of Edwards & Philipp (1985) indicates that the refractive index of diamond, which has no significant optical lattice absorption, is reduced by $\sim$1% from 670 nm to 0 cm^{-1} (i.e., as $\lambda \rightarrow \infty$). We assumed that n for each nitrile we studied was also reduced by $\sim$ 1% over the same range.

The envelope spectrum we calculated included all reflections from the ice–vacuum, the ice–substrate, and the substrate–vacuum interfaces; all interference effects in the film were modeled. As a final consistency check, we compared the envelope spectrum with the measured spectrum. When the film thickness and refractive index were a good match, the phase of the channel fringes in the two traces would agree, with fringe amplitudes also usually matching at the longer wavelengths. An example is given in Figure 2 for HCN. If adequate agreement was not seen, we recalculated the film thickness until the fit was satisfactory which resulted in a thickness generally good to within $\pm$4%. This error propagates to an error in the mid-infrared extinction coefficient of about 4%.

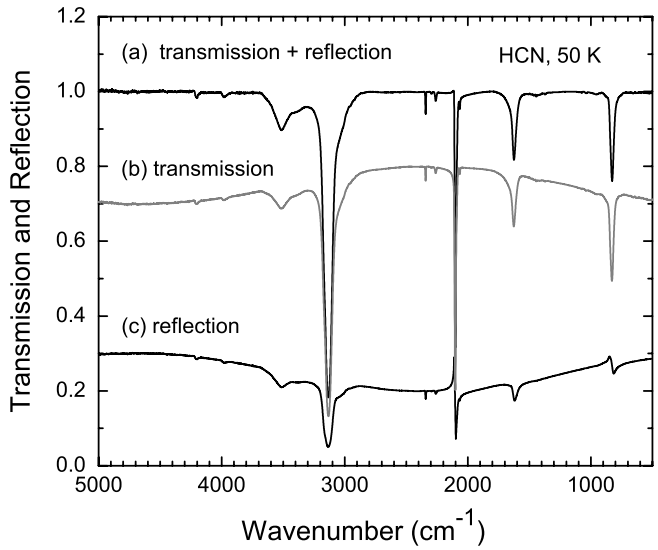

Figure 3. Calculated transmission spectrum of HCN (b) in the mid-infrared at 50 K compared with (c) the corresponding calculated reflection spectrum. The sum of (b) and (c) produces a sum spectrum (a).

Analysis next restored the channel fringes to the baselined spectrum by multiplying it by the calculated envelope spectrum. The product was a close replica of the originally measured transmission data, differing by having fully formed channel fringes and no scattering losses. It was this final "reference" spectrum that was used for subsequent Kramers–Kronig (K-K) analysis.

Initial values for the extinction coefficient, k, and interim values during iteration were determined from the ratio of each interim spectrum to the reference spectrum just described. From this k, a set of n-values was calculated by a K-K transform. We used the Maclaurin K-K algorithm discussed by Ohta & Ishida (1988), which we and others (e.g., Bertie & Zhang 1992) find to be fast and relatively accurate. This algorithm was implemented in Mathcad, but other implementations could be equally efficient.

This first K–K transform provided approximate n- and k-values for the studied nitrile ice; however at this point, we have not yet included the substantial modulation of reflection in the neighborhood of absorption features. We improved the result by iterating the calculation to find a self-consistent n and k set yielding a calculated transmission spectrum that agreed with the reference spectrum. Iterations were continued until the ratio of the calculated spectrum to the reference spectrum deviated from 1 by $< 10^{-5}$ at all wavenumbers. In the mid-infrared region the number of iterations was 15–20 and in the far-infrared it was 40–50. An example of the calculated transmission of a film on its substrate (not ratioed to substrate transmission), its reflectance, and the sum of the two is shown in Figure 3. Significant modulations in reflectance due to refractive index changes at absorption features can be seen.

Close agreement between reference and calculated spectra gave confidence that the n- and k-values derived were representative of the ice studied. In order to check this assumption, we did another test in which n- and k-values were generated by one or more Lorentz oscillators. From these n and k sets a resulting transmission spectrum (T1) was calculated. It was processed using the K-K transform resulting in new n- and k-values and a transmission spectrum (T2). When the ratio of our K-K calculated spectrum T2 to the spectrum T1 deviated from 1 by $<10^{-5}$, the ratio of their corresponding refractive indices deviated from 1 by $\leqslant 0.1$ and their extinction coefficients deviated at their peaks from 1 by $\leqslant 0.05$. These differences, however, appear to be intrinsic to the K-K transform and the conditions of the experiment since we found no significant improvement with additional iterations.

4. RESULTS

Mid- and far-infrared transmission spectra, the refractive index (n), and extinction coefficient (k) for each nitrile are presented here for both crystalline and amorphous phases at several temperatures. Since mid- and far-infrared spectra were acquired in separate experiments with films of different thickness, the optical constants for the two regions required separate calculations. To combine the refractive index data in the region of overlap (650–400 cm^{-1}), the following adjustment was made. The final n was calculated from K-K analysis of the mid-infrared transmission spectrum extrapolated to zero wavenumbers. The zero-wavenumber value was then used as the starting n for the far-infrared region. For data plotted in Figures 4 through 8, the far-infrared n data had to be increased to match the mid-infrared values by adding a small offset, of the order of a few times 0.1% in several cases.

Each material's approximate transmission spectrum is included in our figures to show the pattern of weak and strong absorption features of the molecule. Here, the approximate transmission is calculated from

$$I = I_o \exp(-4\pi k \tilde{\nu}\, d), \tag{3}$$

where k is the extinction coefficient, $\tilde{\nu}$ is the wavenumber in cm^{-1}, and d is the ice film's thickness in cm. Relative intensities of absorptions calculated from Equation (3) do not account for reflection losses. The full modeling approach we used accounts for reflections since both the real and imaginary optical constants were used. This method provided more accurate transmission calculations. In addition to the annealing studies for these nitriles, we show in Section 4.6 two examples where spectra of annealed ices are compared with spectra of crystalline ices formed by directly depositing at the annealing temperature.

The n- and k-values for each nitrile experiment are available electronically as part of the Astrophysical Journal Supplement Series Journal, and also are posted on the Cosmic Ice Laboratory's Web site[5].

4.1. HCN

Spectra of amorphous phase HCN recorded from 5000 to 400 cm^{-1} at 50, 75, 95, and 110 K are shown in Figure 4(a) joined with far-infrared spectra covering the 650 to 30 cm^{-1} region for the same temperatures. The mid-infrared ice film was formed on a KRS-5 substrate by three slow depositions resulting in a gradual buildup of the film thickness to 0.84 μm (determined by a fit of the channel fringes). The mid-infrared spectral resolution was 2 cm^{-1} and optical constants were calculated with one point every 0.5 cm^{-1}. In the far-infrared the film was formed on an HDPE substrate at an average rate of 2.1 μm hr^{-1} to a thickness of 2.6 μm. The spectral resolution was 4 cm^{-1} and optical constants were calculated with one point every 1 cm^{-1}. The measured amorphous phase refractive index at 670 nm was 1.30, and the calculated value at 5000 cm^{-1} was 1.29.

[5] http://science.gsfc.nasa.gov/691/cosmicice

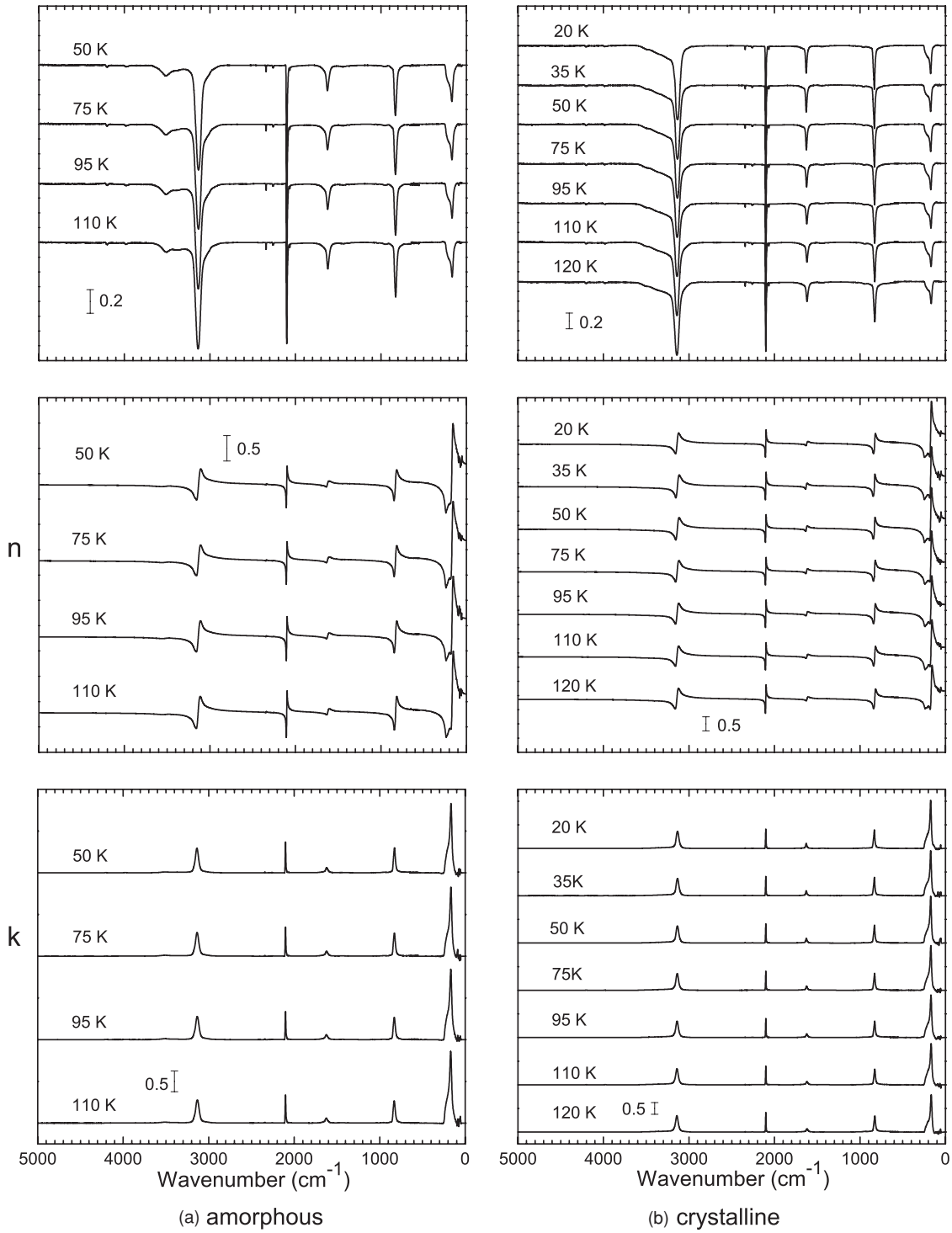

Figure 4. Transmission spectra and optical constants (n and k) of HCN ice in the amorphous phase (a) at temperatures of 50, 75, 95, and 110 K and in the crystalline phase (b) at temperatures of 20, 35, 50, 75, 95, 110, and 120 K. The original HCN ice was deposited at 50 K and annealed at 120 K. A vertical bar indicates the scale, and spectra are stacked for clarity.

Crystalline phase HCN was formed by warming the ice to the 120 K annealing temperature and holding it there for 120 minutes (mid-infrared), and at least 80 minutes (far-infrared) until no further changes were observed. Spectra of crystalline phase HCN recorded from 5000 to 550 cm^{-1} at 120, 110, 95, 75, 50, 35, and 20 K are shown in Figure 4(b) joined together with far-infrared spectra covering the 650 to 30 cm^{-1} region for the same temperatures. The thickness of the crystalline phase ice was 79% that of the amorphous phase. The measured crystalline phase refractive index at 670 nm was 1.39, and the calculated refractive index at 5000 cm^{-1} was 1.37.

4.2. C_2N_2

Spectra of amorphous phase C_2N_2 recorded from 5000 to 400 cm^{-1} at 20, 35, 50, and 75 K are shown in Figure 5(a) with far-infrared spectra covering the 650 to 30 cm^{-1} region for the same temperatures. For this molecule, two different

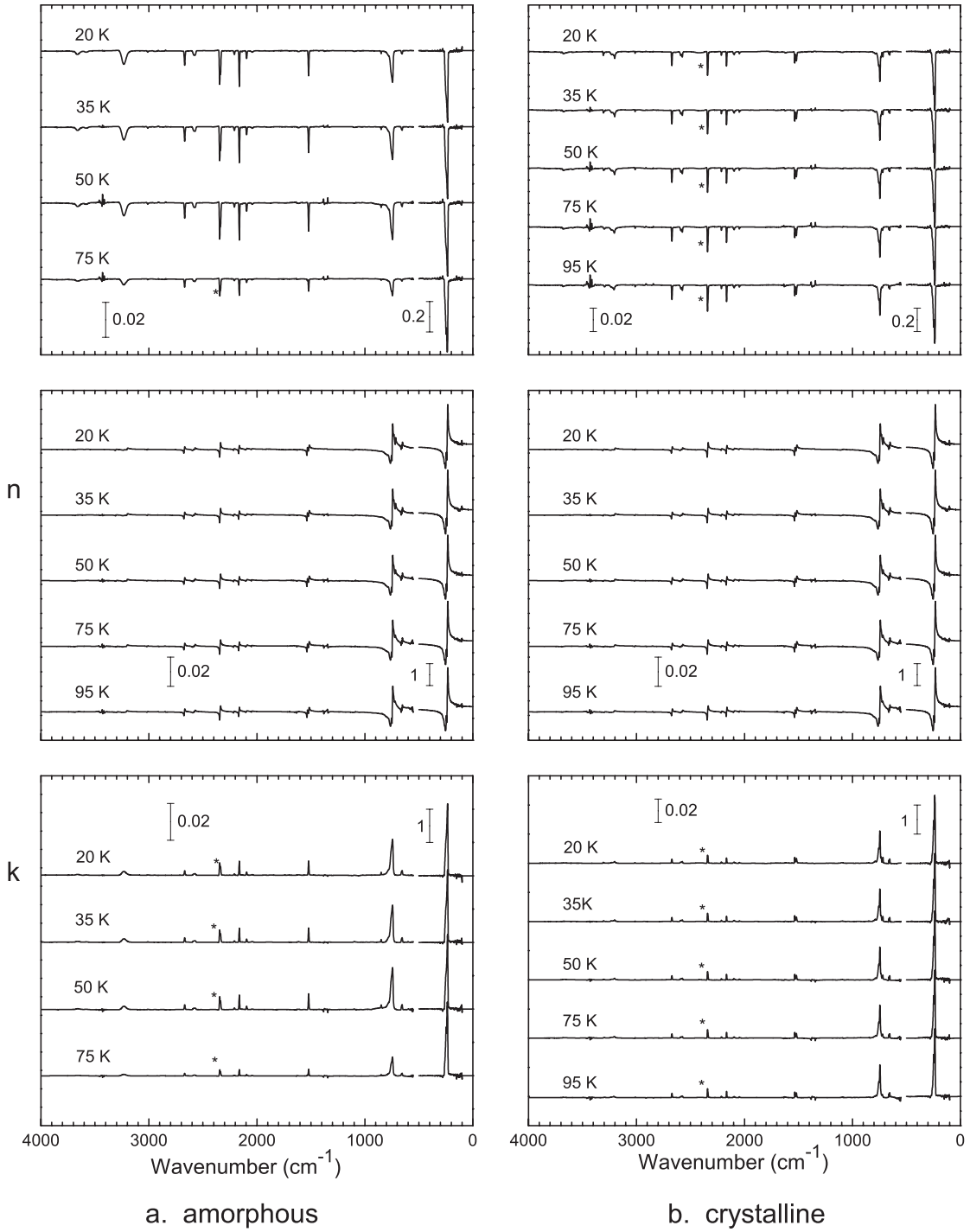

Figure 5. Transmission spectra and optical constants (n and k) of C_2N_2 ice in the amorphous phase (a) at temperatures of 20, 35, 50, and 75 and in the crystalline phase (b) at temperatures of 20, 35, 50, 75, and 95 K. The original C_2N_2 ice was deposited at 20 K and annealed at 95 K. A vertical bar indicates the scale, and spectra are stacked for clarity. The mid- and far-infrared segments have different scale bars.

scales are used for the mid- and far-infrared spectra. In the mid-infrared experiment, the ice film was made on a CsI substrate at a rate of 6.4 μm hr^{-1} to a thickness of 3.85 μm. The mid-infrared spectral resolution was 4 cm^{-1} and optical constants were calculated with one point every 1 cm^{-1}. In the far-infrared, the film was formed on an HDPE substrate at an average rate of 2.57 μm hr^{-1} to a thickness of 1.54 μm. The spectral resolution was 4 cm^{-1} and optical constants were calculated with one point every 1 cm^{-1}. The measured amorphous phase refractive index at 670 nm was 1.30, and the calculated value at 5000 cm^{-1} was 1.29.

Crystalline phase C_2N_2 was formed by warming the ice to the 90 K annealing temperature and holding it there for 60 minutes (mid-infrared), and ~90 minutes (far-infrared) until no further changes were observed. Spectra of crystalline phase C_2N_2 recorded from 4000 to 550 cm^{-1} at 90 (but, for consistency, plotted in Figure 5(b) with a temperature of 95 K), 75, 50, 35, and 20 K are shown in Figure 5(b) joined with far-infrared spectra covering the 650 to 30 cm^{-1} region for the same temperatures. The thickness of the crystalline phase ice was 96% that of the amorphous phase. The measured crystalline phase refractive

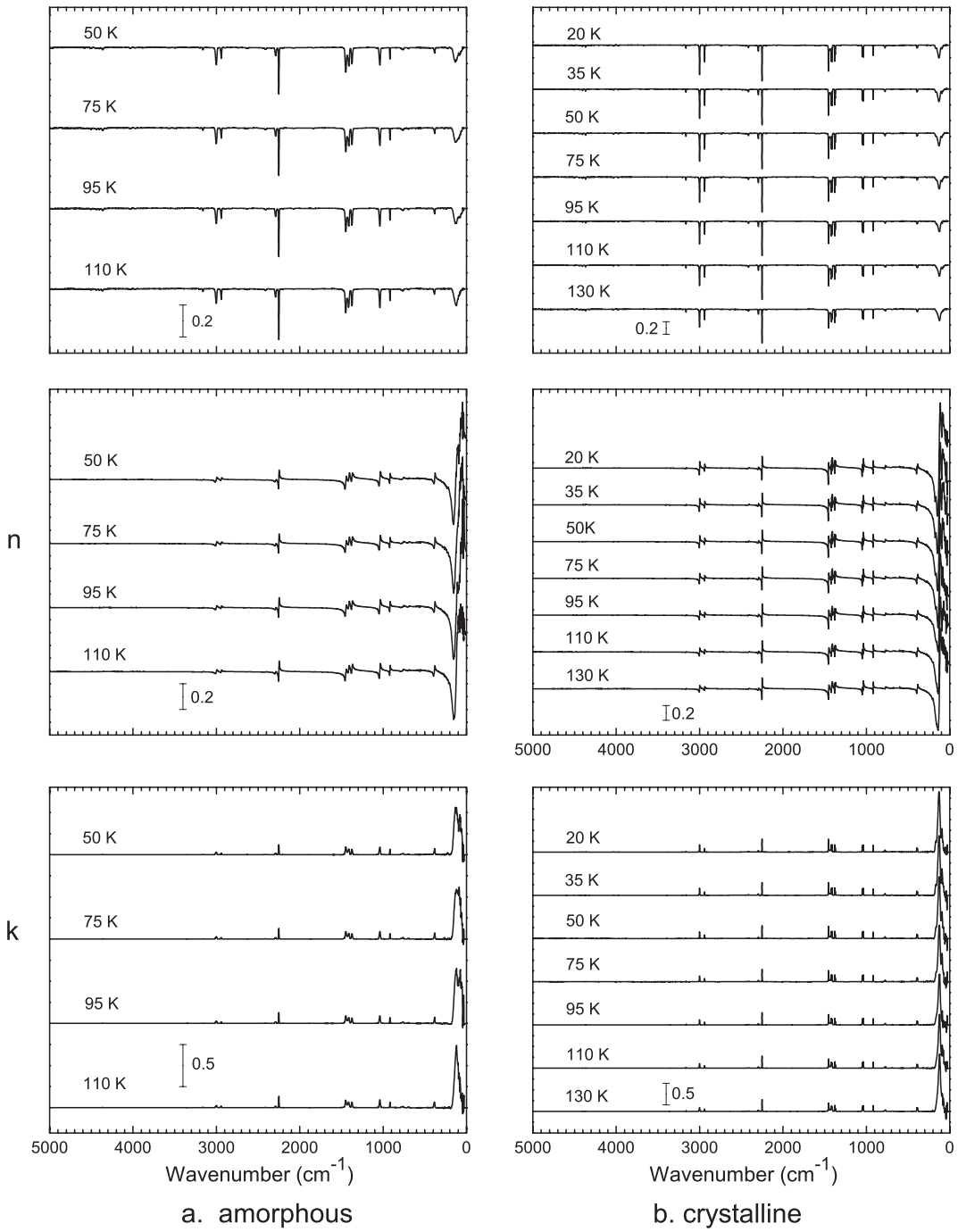

Figure 6. Transmission spectra and optical constants (n and k) of CH_3CN ice in the amorphous phase (a) at temperatures of 50, 75, 95, and 110 K and in the crystalline phase (b) at temperatures of 20, 35, 50, 75, 95, 110, and 130 K. The original CH_3CN ice was deposited at 50 K and annealed at 130 K. A vertical bar indicates the scale, and spectra are stacked for clarity.

index at 670 nm was 1.42, and the calculated refractive index at 5000 cm^{-1} was 1.40.

4.3. CH_3CN

Spectra of amorphous phase CH_3CN recorded from 5000 to 400 cm^{-1} at 50, 75, 95, and 110 K are shown in Figure 6(a) joined together with far-infrared spectra covering the 650 to 30 cm^{-1} region for the same temperatures. In the mid-infrared experiment, the ice film was made on a KRS-5 substrate at a rate of 11.9 μm hr^{-1} to a total thickness of 1.39 μm. The mid-infrared spectral resolution was 2 cm^{-1} and optical constants were calculated with one point every 0.5 cm^{-1}. In the far-infrared the film was formed on an HDPE substrate at a rate of 7.67 μm hr^{-1} to a thickness of 2.8 μm. The spectral resolution was 4 cm^{-1} and optical constants were calculated with one point every 1 cm^{-1}. The measured amorphous phase refractive index at 670 nm was 1.31 and the calculated value at 5000 cm^{-1} was 1.30.

Crystalline phase CH_3CN was formed by warming the ice to the 130 K annealing temperature and holding it there for 66 minutes (mid-infrared), and ~45 minutes (far-infrared) until no further changes were observed. Spectra of annealed crystalline phase CH_3CN recorded from 5000 to 550 cm^{-1} at 130, 110, 95, 75, 50, 35, and 20 K are shown in Figure 6(b)

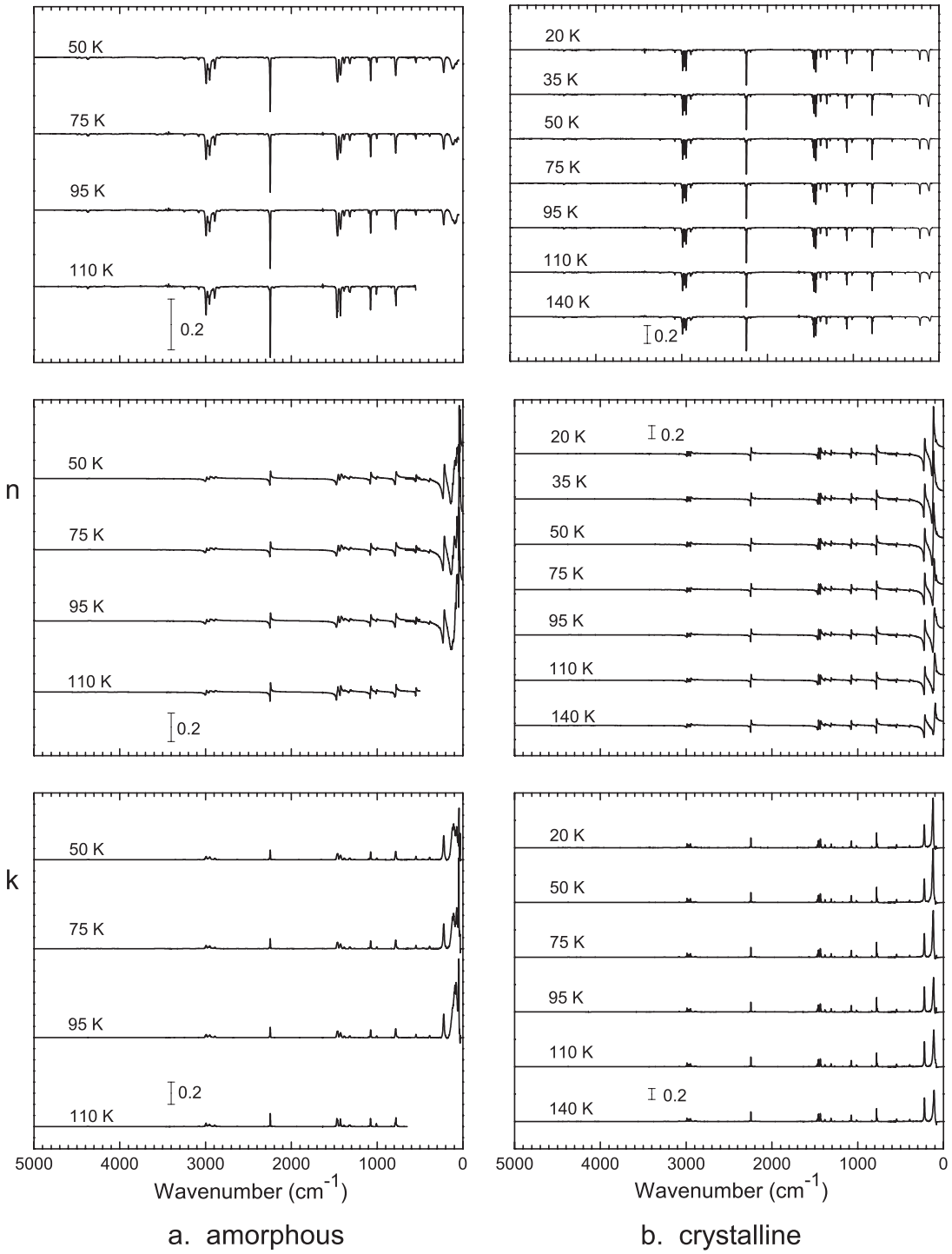

Figure 7. Transmission spectra and optical constants (n and k) of C_2H_5CN ice in the amorphous phase (a) at temperatures of 50, 75, 95, and 110 K and in the crystalline phase (b) at temperatures of 20, 35, 50, 75, 95, 110, and 140 K. The original C_2H_5CN ice was deposited at 50 K and annealed at 140 K. A vertical bar indicates the scale, and spectra are stacked for clarity.

joined with far-infrared spectra covering the 650 to 30 cm^{-1} region for the same temperatures. The thickness of the annealed crystalline phase ice was 89% that of the amorphous phase. The measured crystalline phase refractive index at 670 was 1.45, and the calculated refractive index at 5000 cm^{-1} was 1.41.

4.4. C_2H_5CN

Spectra of amorphous phase C_2H_5CN recorded from 5000 to 400 cm^{-1} at 50, 75, 95, and 110 K are shown in Figure 7(a) joined together with far-infrared spectra covering the 650 to 30 cm^{-1} region for the same temperatures. In the mid-infrared experiment, the ice film was made on a CsI substrate at a rate of 8.6 μm hr^{-1} to a total thickness of 2.29 μm. The mid-infrared spectral resolution was 2 cm^{-1} and optical constants were calculated with one point every 0.5 cm^{-1}. In the far-infrared the film was formed on an HDPE substrate at a rate of 15.9 μm hr^{-1} to a thickness of 5.3 μm. The spectral resolution was 4 cm^{-1} and optical constants were calculated with one point every 1 cm^{-1}. The measured amorphous phase refractive

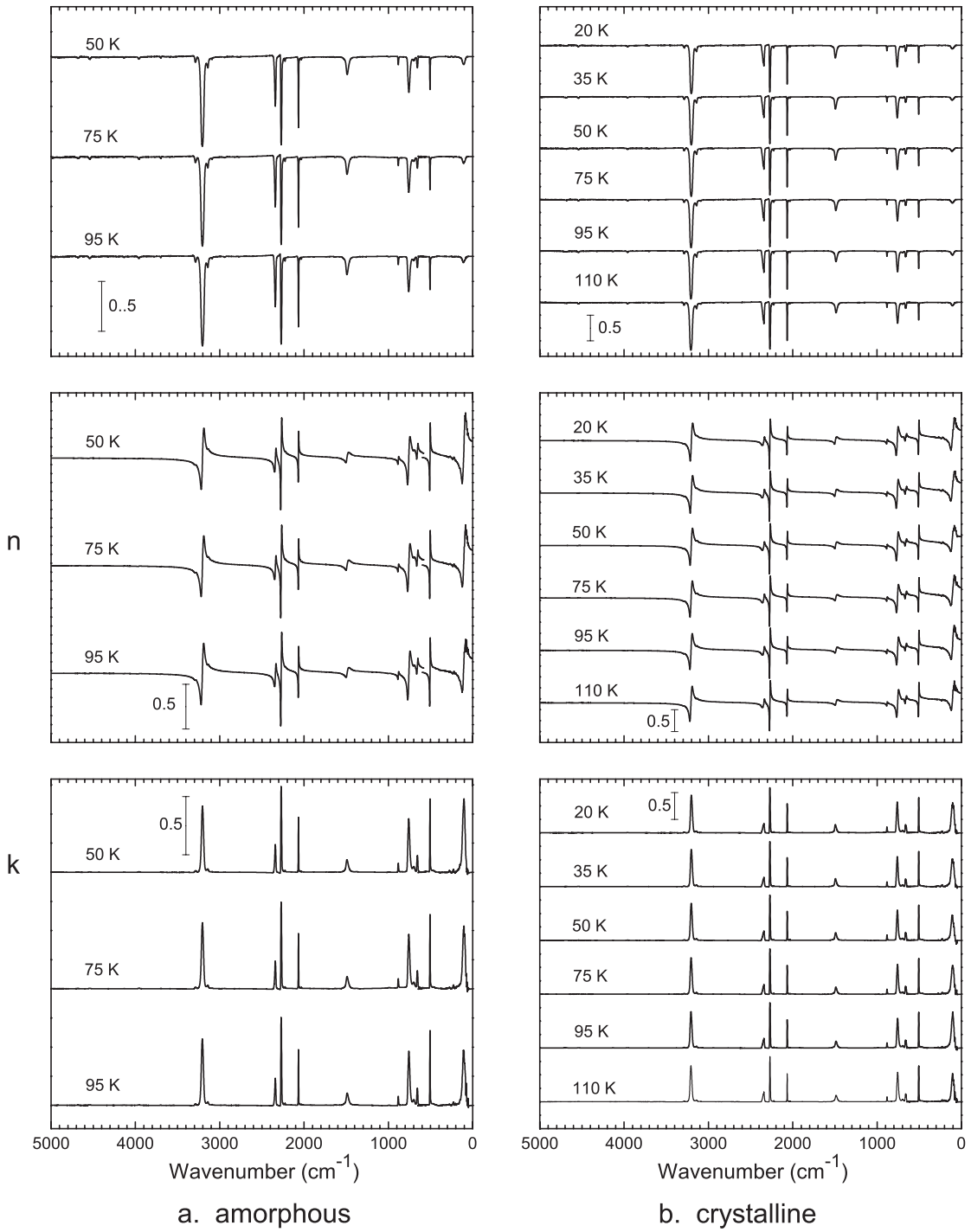

Figure 8. Transmission spectra and optical constants (n and k) of HC_3N ice in the amorphous phase (a) at temperatures of 50, 75, and 95 K and in the crystalline phase (b) at temperatures of 20, 35, 50, 75, 95, and 110 K. The original HC_3N ice was deposited at 50 K and annealed at 110 K. A vertical bar indicates the scale, and spectra are stacked for clarity.

index at 670 nm was 1.26, and the calculated refractive index at 5000 cm^{-1} was 1.25.

Crystalline phase C_2H_5CN was formed by warming the ice to the 140 K annealing temperature and holding it there for 90 minutes (mid-infrared), and 92 minutes (far-infrared). Spectra of crystalline phase C_2H_5CN recorded from 5000 to 550 cm^{-1} at 140, 110, 95, 75, 50, 35, and 20 K are shown in Figure 7(b) joined with far-infrared spectra covering the 650 to 30 cm^{-1} region for the same temperatures. The thickness of the crystalline phase ice was 76% that of the amorphous phase. The measured crystalline phase refractive index at 670 nm was 1.49, and the calculated refractive index at 5000 cm^{-1} was 1.47.

4.5. HC_3N

Spectra of amorphous phase HC_3N recorded from 5000 to 400 cm^{-1} at 50, 75, and 95 K are shown in Figure 8(a) joined together with far-infrared spectra covering the 650 to 30 cm^{-1} region for the same temperatures. In the mid-infrared experiment, the ice film was made on a KRS-5 substrate at a

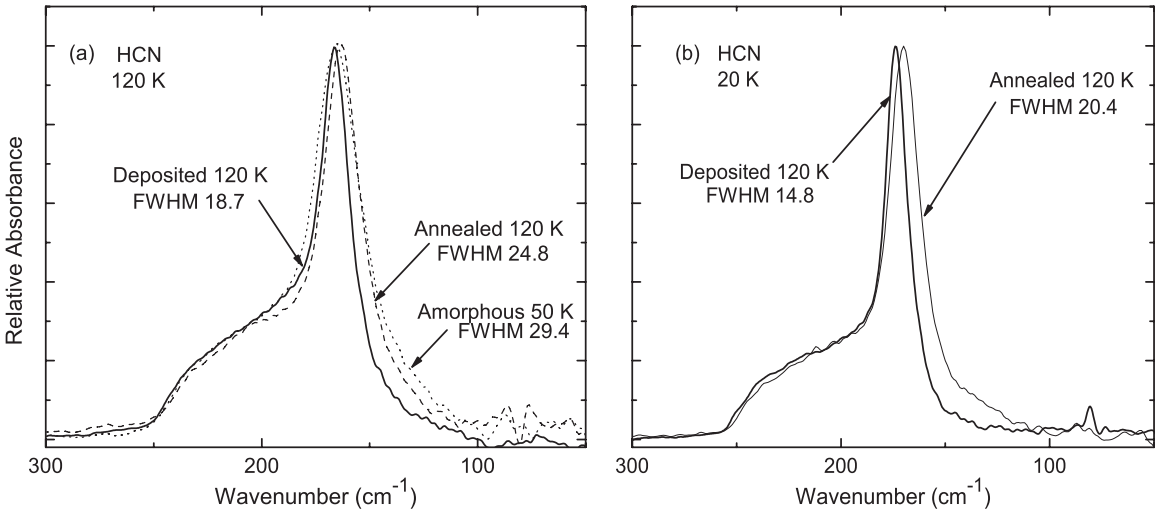

Figure 9. (a) Far-infrared spectra of amorphous-phase HCN and that same ice annealed to 120 K are compared with a spectrum of HCN formed directly at 120 K. (b) The widths of the HCN bands are shown for ices cooled to 20 K.

rate of 1.5 μm hr^{-1} to a total thickness of 0.64 μm. The mid-infrared spectral resolution was 2 cm^{-1} and optical constants were calculated with one point every 0.5 cm^{-1}. In the far-infrared the film was formed on an HDPE substrate at a rate of 15.6 μm hr^{-1} to a total thickness of 3.12 μm. The spectral resolution was 4 cm^{-1} and optical constants were calculated with one point every 1 cm^{-1}. The measured amorphous phase refractive index at 670 nm was 1.41, and the calculated refractive index at 5000 cm^{-1} was 1.38.

Crystalline phase HC_3N was formed by warming the ice to the 110 K annealing temperature and holding it there for 120 minutes (mid-infrared) and $\sim$ 65 minutes (far-infrared) until no further changes were observed. Spectra of crystalline phase HC_3N recorded from 5000 to 550 cm^{-1} at 110, 95, 75, 50, 35, and 20 K are shown in Figure 8(b) joined with far-infrared spectra covering the 650 to 30 cm^{-1} region for the same temperatures. The thickness of the crystalline phase ice was 98% that of the amorphous phase. The measured crystalline phase refractive index at 670 nm was 1.43 and the calculated refractive index at 5000 cm^{-1} was 1.41.

4.6. Annealed versus Deposited Crystalline Ices

Far-infrared spectra of HCN are compared in Figure 9(a) for a 0.7 μm thick HCN ice, grown at 50 K (amorphous phase) and warmed to 120 K (crystalline phase), and an $\sim$1.75 μm HCN ice formed directly on a 120 K substrate (deposited crystalline phase). The bands are normalized to have the same maximum peak intensity. Figure 9(b) shows the same spectra for those ices cooled to 20 K where each peak position has shifted to higher energy by about 7 cm^{-1} and each has a smaller FWHM by about 4 cm^{-1}.

Mid-infrared spectra of C_2H_5CN are compared in Figure 10 for (a) an amorphous phase deposit at 50 K, (b) that same ice warmed to 140 K and held for 90 minutes, and (c) for C_2H_5CN deposited directly onto the 140 K substrate. Each spectrum was recorded at a resolution of 2 cm^{-1} and the ice thickness was $\sim$1.25 μm. The broader amorphous phase bands sharpen and, in some cases, split with annealing. Contrasting the spectrum of the ice that was warmed to 140 K (b) with the spectrum of the ice deposited at 140 K (c), differences in peak profiles and relative band intensities are found. The ν_8 CH_2 wag feature in (c) is split, but not in spectrum (b). Band shifts to higher energy,

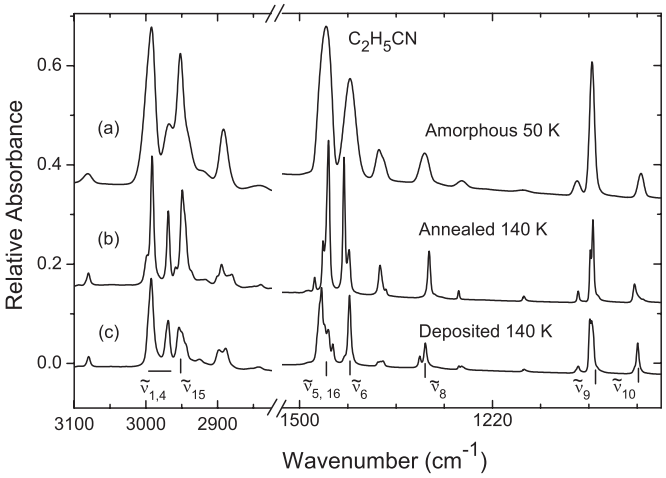

Figure 10. Regions of the mid-infrared spectrum of C_2H_5CN are compared for (a) an amorphous phase deposit at 50 K, (b) that same ice annealed at 140 K, and (c) for C_2H_5CN deposited directly onto the 140 K substrate. Spectra are stacked for clarity. Vibrational assignments are based on Crowder (1986).

as large as 10 cm^{-1} for the strongest absorptions near 1500 and 1427 cm^{-1} (ν_5, ν_{16}, and ν_6), are found in spectrum (c). Not shown in Figure 10 are minor changes in the 2254 cm^{-1} (C$\equiv$N stretch) absorption, the strongest feature of the C_2H_5CN spectrum.

5. MACHINE-READABLE TABLES

We include machine-readable tables. For each nitrile there is tabulation of *n*- and of *k*-values calculated for each temperature shown in Figures 4 through 8 for the amorphous and the crystalline phase of each nitrile. Tables 3(a)–(e) have *n*-values for amorphous phase ices; Tables 4(a)–(e) have *k*-values for amorphous phase ices; Tables 5(a)–(e) have *n*-values for crystalline phase ices; and Tables 6(a)–(e) have *k*-values for crystalline phase ices. All tabulated values for crystalline ices are for annealed ices, not those that were directly deposited. Tables 3(a)–(e) refer to molecules HCN, C_2N_2, CH_3CN, C_2H_5CN, and HC_3N, respectively. A similar structure is used for Tables 4(a)–(d), 5(a)–(d), and 6(a)–(d). Stub tables in this paper contain the first five lines for each of the online tables. The stub tables are Tables 3–6. The full

Table 3
Index of Refraction (n)—Amorphous Phase Nitriles

	Molecule	Wavenumber (cm^{-1})	50 K	75 K	95 K	110 K
(a)	HCN	5000.00	1.28600	1.28600	1.28600	1.28600
		4999.50	1.27980	1.28035	1.27735	1.27889
		4999.00	1.27960	1.28019	1.27718	1.27865
		4998.50	1.27962	1.28010	1.27739	1.27862
		4998.00	1.27963	1.28018	1.27744	1.27856
(b)	C_2N_2	4000.00	1.28980	1.2898	...	...
		3999.00	1.28958	1.28965	...	...
		3998.00	1.28958	1.28965	...	...
		3997.00	1.28959	1.28966	...	...
		3996.00	1.28959	1.28966	...	...
(c)	CH_3CN	5000.00	1.29550	1.29550	1.29550	1.29550
		4999.50	1.29460	1.29439	1.29403	1.29412
		4999.00	1.29455	1.29439	1.29406	1.29423
		4998.50	1.29458	1.29446	1.29415	1.29440
		4998.00	1.29469	1.29451	1.29428	1.29454
(d)	C_2H_5CN	5000.00	1.24725	1.24720	1.24710	1.24715
		4999.50	1.24724	1.24720	1.24710	1.24715
		4999.00	1.24724	1.24720	1.24709	1.24715
		4998.50	1.24724	1.24720	1.24708	1.24715
		4998.00	1.24724	1.24720	1.24708	1.24715
(e)	HC_3N	5000.00	1.37183	1.37154	1.37042	...
		4999.50	1.37184	1.37119	1.37023	...
		4999.00	1.37187	1.37088	1.37031	...
		4998.50	1.37190	1.37074	1.37053	...
		4998.00	1.37194	1.37079	1.37075	...

(This table is available in its entirety in a machine-readable form in the online journal. A portion is shown here for guidance regarding its form and content.)

n- and k-tables may be requested from the corresponding author, or found in the online version of the journal and the Cosmic Ice Web site at.[5]

6. DISCUSSION

The spectral properties of ices between 1000 and 200 cm^{-1} are of interest for comparison with Titan's *Voyager* data, and those extending to 30 cm^{-1} are valuable for comparing with *Cassini* data. As an example of an outstanding problem, the source of the towering 220 cm^{-1} emission feature of the winter pole of Titan is not known, and it has been shown that it is not compatible with pure crystalline C_2H_5CN at 95 K (see Samuelson et al. 2007). Another observational feature that is unidentified is the emission feature near 160 cm^{-1} seen at 15 S and 15 N in Titan's stratosphere (Samuelson & Anderson 2009). This emission feature occurs between 60 and 100 km, an altitude where many nitriles are expected to condense. Figure 11 is a plot of the derived "ice" opacity of this feature after removing the aerosol component (Samuelson & Anderson 2009). Transmission spectra of several crystalline-phase nitriles measured in our laboratory at 95 K are compared with the broad emission feature. It is thought that the shape of the feature is best fit with a combination of nitriles such as the ones shown here. The laboratory data presented in this paper provide a set of optical constants for both the amorphous and crystalline phases of several relevant nitriles at a variety of temperatures. These data provide new information that can be used to address the temperature dependence of band positions, intensities, and band shapes that can be used to model observational features.

In two cases, we have compared the spectra of annealed ice with those directly condensed at the annealing temperature to look at changes in band positions and band shape. Figure 9(a) shows some small differences between the far-infrared spectra of HCN at 120 K formed with these two different techniques. The peak position for annealed HCN is at a lower energy than for HCN directly deposited at 120 K. The annealed HCN has

Table 4
Extinction Coefficient (k)—Amorphous Phase Nitriles

	Molecule	Wavenumber (cm^{-1})	50 K	75 K	95 K	110 K
(a)	HCN	5000.00	1.04019E-04	−4.49112E-04	7.63172E-04	2.45897E-04
		4999.50	−2.22256E-04	−6.43544E-04	5.01981E-04	−8.28765E-05
		4999.00	−2.59002E-04	−6.16186E-04	5.36868E-04	−1.19781E-04
		4998.50	−2.39791E-04	−5.24114E-04	5.70710E-04	−7.36613E-05
		4998.00	−2.51373E-04	−4.50899E-04	5.49199E-04	9.70203E-06
(b)	C_2N_2	4000.00	4.63710E-05	4.70645E-05	...	...
		3999.00	4.95912E-05	4.93923E-05	...	...
		3998.00	5.19205E-05	4.96761E-05	...	...
		3997.00	5.29646E-05	4.91597E-05	...	...
		3996.00	5.35859E-05	4.88093E-05	...	...
(c)	CH_3CN	5000.00	−4.21616E-05	1.09513E-04	4.75214E-05	1.50686E-04
		4999.50	2.67394E-05	1.64193E-04	2.26330E-04	3.54233E-04
		4999.00	1.43696E-04	2.22548E-04	3.81603E-04	4.86498E-04
		4998.50	2.97175E-04	2.77941E-04	5.16513E-04	5.37270E-04
		4998.00	3.90203E-04	2.66230E-04	5.71323E-04	4.82259E-04
(d)	C_2H_5CN	5000.00	−9.75649E-05	3.63752E-05	−4.09490E-06	7.56768E-05
		4999.50	−9.88663E-05	3.14573E-05	−8.17777E-06	7.09402E-05
		4999.00	−9.80801E-05	2.65591E-05	−9.39807E-06	6.82151E-05
		4998.50	−9.80277E-05	2.10027E-05	−9.92318E-06	6.62037E-05
		4998.00	−9.79906E-05	1.69102E-05	−7.58281E-06	6.48901E-05
(e)	HC_3N	5000.00	5.44233E-04	9.25452E-04	4.48971E-05	...
		4999.50	6.05576E-04	8.27140E-04	4.07587E-04	...
		4999.00	6.46163E-04	1.00000E-03	7.79987E-04	...
		4998.50	6.70726E-04	1.30000E-03	9.86397E-04	...
		4998.00	6.32194E-04	1.57000E-03	1.04000E-03	...

(This table is available in its entirety in a machine-readable form in the online journal. A portion is shown here for guidance regarding its form and content.)

Table 5
Index of Refraction (n)—Crystalline Phase Nitriles

	Molecule	Wavenumber (cm^{-1})	20 K	35 K	50 K	75 K	95 K	110 K	T (K)[a]
(a)	HCN	5000.00	1.37200	1.37200	1.37200	1.37200	1.37200	1.37200	1.37200
		4999.50	1.36247	1.36138	1.36257	1.36311	1.36258	1.36510	1.36190
		4999.00	1.36264	1.36161	1.36283	1.36326	1.36287	1.36522	1.36232
		4998.50	1.36280	1.36182	1.36311	1.36321	1.36294	1.36504	1.36251
		4998.00	1.36297	1.36197	1.36333	1.36314	1.36295	1.36517	1.36269
(b)	C_2N_2	4000.00	1.40260	1.40260	1.4026	1.40260	1.4026	...	...
		3999.00	1.40251	1.40250	1.40254	1.40232	1.40249	...	...
		3998.00	1.40251	1.40250	1.40254	1.40232	1.4025	...	...
		3997.00	1.40251	1.40250	1.40255	1.40235	1.4025	...	...
		3996.00	1.40250	1.40250	1.40254	1.40234	1.40249	...	...
(c)	CH_3CN	5000.00	1.43000	1.43000	1.43000	1.43000	1.43000	1.43000	1.43000
		4999.50	1.42828	1.42879	1.42842	1.42926	1.42867	1.42813	1.42838
		4999.00	1.42840	1.42885	1.42848	1.42930	1.42867	1.42814	1.42833
		4998.50	1.42854	1.42893	1.42851	1.42932	1.42865	1.42823	1.42830
		4998.00	1.42872	1.42903	1.42863	1.42939	1.42874	1.42839	1.42836
(d)	C_2H_5CN	5000.00	1.46783	1.46786	1.46792	1.46789	1.46792	1.46789	1.46783
		4999.50	1.46782	1.46785	1.46792	1.46790	1.46792	1.46789	1.46783
		4999.00	1.46783	1.46784	1.46791	1.46789	1.46792	1.46789	1.46784
		4998.50	1.46783	1.46784	1.46791	1.46789	1.46792	1.46788	1.46784
		4998.00	1.46784	1.46783	1.46791	1.46788	1.46791	1.46788	1.46784
(e)	HC_3N	5000.00	1.41350	1.41350	1.4135	1.41350	1.4135	1.41350	...
		4999.50	1.40497	1.40552	1.40586	1.40710	1.40744	1.40684	...
		4999.00	1.40520	1.40565	1.40589	1.40721	1.40772	1.40695	...
		4998.50	1.40543	1.40584	1.40590	1.40715	1.40783	1.40692	...
		4998.00	1.40568	1.40613	1.40605	1.40738	1.40811	1.40707	...

Note. [a] HCN (120 K), CH_3CN (130 K), C_2H_5CN(140 K).

(This table is available in its entirety in a machine-readable form in the online journal. A portion is shown here for guidance regarding its form and content.)

Table 6
Extinction Coefficient (k)–Crystalline Phase Nitriles

	Molecule	Wavenumber (cm^{-1})	20 K	35 K	50 K	75 K	95 K	110 K	T (K)[a]
(a)	HCN	5000.00	7.00362E-04	1.01797E-03	9.29354E-04	4.27034E-04	1.87604E-04	−7.46556E-04	2.61106E-04
		4999.50	9.95511E-04	1.30127E-03	1.27804E-03	5.83667E-04	4.60461E-04	−5.08214E-04	7.39524E-04
		4999.00	1.01167E-03	1.23825E-03	1.30160E-03	3.76962E-04	3.43595E-04	−5.10207E-04	7.42630E-04
		4998.50	1.08430E-03	1.22305E-03	1.33244E-03	2.63233E-04	1.74545E-04	−4.47819E-04	6.27896E-04
		4998.00	1.14886E-03	1.19519E-03	1.29503E-03	2.71226E-04	−3.23274E-05	−3.94601E-04	4.43348E-04
(b)	C_2N_2	4000.00	−2.86068E-06	4.17921E-06	3.02015E-05	1.28404E-04	1.71063E-05	...	...
		3999.00	−8.13185E-06	−5.82455E-07	2.48158E-05	1.18181E-04	1.25148E-05	...	...
		3998.00	−1.61377E-05	−6.39547E-06	1.65231E-05	1.08949E-04	3.12788E-06	...	...
		3997.00	−2.53643E-05	−1.38846E-05	7.03617E-06	9.78366E-05	−8.53042E-06	...	...
		3996.00	−3.13820E-05	−1.98484E-05	−1.21900E-06	8.78035E-05	−1.62286E-05	...	...
(c)	CH_3CN	5000.00	3.54119E-05	8.53126E-05	−7.30404E-05	−9.65368E-05	−1.26385E-04	3.25626E-04	7.48796E-05
		4999.50	2.73830E-04	1.76348E-04	8.69531E-05	−6.82286E-06	−8.90520E-06	4.44736E-04	1.01410E-04
		4999.00	4.07958E-04	2.14800E-04	1.63652E-04	5.36982E-05	5.90750E-05	5.23611E-04	1.12917E-04
		4998.50	4.95131E-04	2.42439E-04	2.44803E-04	1.01782E-04	1.76359E-04	6.56357E-04	2.18799E-04
		4998.00	4.60272E-04	1.88096E-04	2.60855E-04	9.42935E-05	2.58358E-04	7.32969E-04	3.10270E-04
(d)	C_2H_5CN	5000.00	8.70402E-05	5.80482E-05	1.15319E-05	5.63413E-05	2.38575E-05	1.58387E-05	2.52071E-05
		4999.50	9.05186E-05	4.74880E-05	6.26322E-06	4.91104E-05	1.93644E-05	1.04587E-05	2.40879E-05
		4999.00	9.38742E-05	4.31585E-05	6.27528E-06	4.11101E-05	1.66646E-05	5.98405E-06	2.03339E-05
		4998.50	9.27501E-05	4.23311E-05	8.84563E-06	3.58477E-05	1.48400E-05	1.53171E-06	1.48635E-05
		4998.00	8.63528E-05	4.41018E-05	9.53734E-06	3.50310E-05	1.47848E-05	−1.99179E-06	9.45944E-06
(e)	HC_3N	5000.00	7.28719E-04	5.75953E-04	1.22902E-04	−5.59059E-04	−3.94287E-04	−3.75795E-04	...
		4999.50	1.26000E-03	9.86520E-04	4.56210E-04	−1.12218E-04	1.07442E-04	−3.73911E-05	...
		4999.00	1.46000E-03	1.15000E-03	6.28634E-04	1.43425E-04	3.06786E-04	1.22473E-04	...
		4998.50	1.65000E-03	1.36000E-03	8.71926E-04	4.14985E-04	3.97567E-04	2.72794E-04	...
		4998.00	1.72000E-03	1.42000E-03	1.05000E-03	5.90818E-04	2.99120E-04	3.10863E-04	...

Note. [a] HCN (120 K), CH_3CN (130 K), C_2H_5CN(140 K).

(This table is available in its entirety in a machine-readable form in the online journal. A portion is shown here for guidance regarding its form and content.)

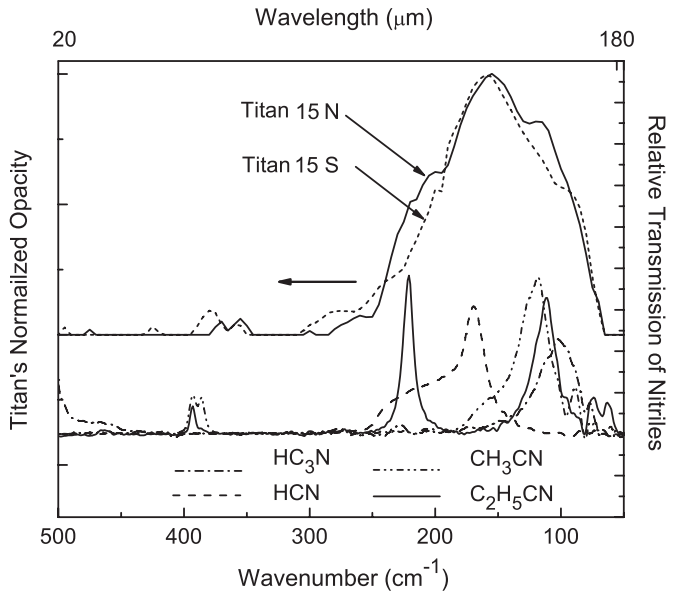

Figure 11. Broad Titan emission feature (Samuelson & Anderson 2009) compared with infrared spectra of possible nitrile ice constituents. Nitrile ice transmission spectra are offset from the opacity plot of the emission feature for clarity.

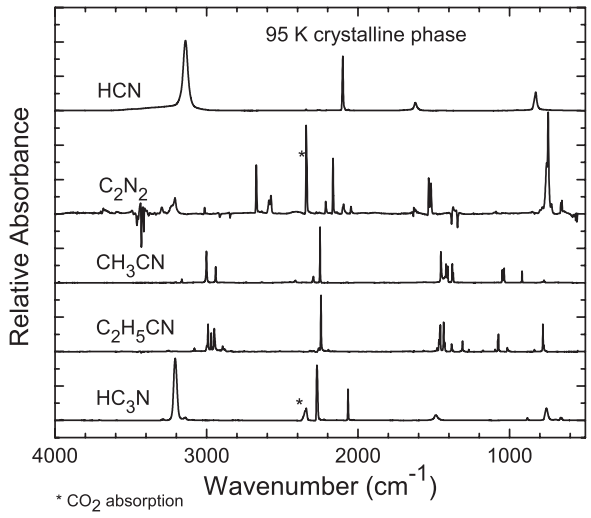

Figure 12. Absorbance spectra of five crystalline phase nitriles at 95 K are compared. Spectra are normalized to the C≡N stretch absorption in the 2100–2200 cm^{-1} region and are stacked for clarity.

a larger FWHM than the ice directly deposited. These same ices retain their relative band positions when cooled to 20 K and each has a smaller FWHM as shown in Figure 9(b). In our experiments, annealing times and temperatures were similar to those reported in Dello Russo & Khanna (1996). HCN is a small linear molecule with hydrogen-bonded chains pointing in the same direction in the crystalline phase (Dulmage & Lipscomb 1951). The far-infrared absorption is due to two lattice modes, both librational. Our HCN comparison experiment suggests that complete ordering of the ice does not occur with 120 K annealing.

The mid-infrared spectral differences found between the annealed and directly deposited (quenching of gas at the annealing temperature) C_2H_5CN at 140 K, shown in Figure 10, also illustrate the difficulty of annealing amorphous films. The annealing times and temperatures we chose were comparable to those of Dello Russo & Khanna (1996), and our results are very similar to their published data. However, they too noted the fact that this molecule required a "greater amount of time" to anneal, and even then, our results show that line splittings were different in the annealed sample compared to an ice film formed at that same temperature. Khanna (2005a) pointed out that CH_2 and CH_3 groups in organic molecules have low barriers to rotation around single bonds and therefore can be difficult to anneal. While variable line splittings apply only to C_2H_5CN, we found that some minor differences between the annealed and high temperature deposits were evident in all of our nitrile samples.

Annealing to attain a good stable crystalline phase requires reorientation of the molecules. For each nitrile ice we have compared both mid- and far-infrared spectra from high-temperature deposits with corresponding spectra after annealing. We conclude that quenching gas-phase molecules at their annealing temperature can produce a more-ordered ice than is possible to attain through reordering of the bulk amorphous-phase material, since an amorphous fraction may remain. Similarly, Sandford & Allamandola (1990) illustrated that deposition of H_2O:CO_2 ices at 90 K resulted in a more ordered ice (narrower bands) than the one deposited at 10 K and subsequently warmed to 90 K. We also know that in all cases the nitrile ices in this study, after annealing, were completely evolved to a final state of order that was not changed with increased annealing time. In most cases, increased time at the annealing temperature led to sublimation.

Studies of quenched nitriles are relevant to the type of ice thought to be forming in the upper atmosphere of Titan. Gas-phase nitriles are transported from higher altitudes, where they are created, down to the mid and lower stratosphere. Condensation occurs in the stratosphere near 140 km. Therefore, studies of ices formed at these higher temperatures may be more relevant to modeling stratospheric ice clouds on Titan. We have seen that spectra of quenched nitriles can display slightly different band positions and shapes. Analysis of these ices is left for a future study of high-temperature deposits.

One case of a dramatic difference between the mid- and far-infrared absorption intensities is worth noting. The far-IR lattice band absorption feature of C_2N_2 has an integrated absorbance value about 20 times that of its strongest mid-IR feature. Comparing the far- and mid-infrared-integrated absorption coefficients (α_{int}) for 35 K crystalline phase C_2N_2 we find (1) in the far-infrared, the absorbance spectrum for the 234.6 cm^{-1} C_2N_2 ν_5 band integrated from 300 to 200 cm^{-1} for a thickness of 1.48 μm gives $\alpha_{int} = 1.3 \times 10^5$ cm^{-2}; (2) in the mid-IR, the absorbance spectrum for the 746 cm^{-1} ($\nu_4 + \nu_5$) C_2N_2 band integrated from 778 to 725 cm^{-1} for a thickness of 3.68 μm gives $\alpha_{int} = 3.7 \times 10^3$ cm^{-2}. Previously published values by Dello Russo & Khanna (1996) give similar 35 K values: ν_5 $\alpha_{int} = 1.1 \times 10^5$ cm^{-2} and $\nu_4 + \nu_5$ $\alpha_{int} = 5.5 \times 10^3$ cm^{-2}.

Figure 12 shows the spectra of all five crystalline nitriles, normalized to the C≡N band in the 2200 cm^{-1} region, from 4000 to 500 cm^{-1}. For HCN, C_2N_2, or HC_3N there are features that are stronger. For HCN and HC_3N the CH stretch is the dominant band, whereas for C_2N_2 it is the $\nu_4 + \nu_5$ combination CCN stretch band. The same set of spectra is shown in Figure 13 plotted for a 1 μm thick ice. This plot compares the relative band strengths of the nitriles and shows that the CH stretch of HCN and HC_3N has the largest intrinsic intensities, whereas the bands of C_2N_2 all have the smallest strengths within this wavelength region.

Table 7
Integrated Absorption Coefficients (α_{int}) of Crystalline Phase Nitriles in the 300–30 cm^{-1} Region Compared to Dello Russo & Khanna (1996)

Molecule	Temp. (K)	Peak Position (cm^{-1})	Mode	Limits of Integration (cm^{-1})	α_{int} (cm^{-2})[a]	α_{int} (cm^{-2})[b]
Dello Russo & Khanna (1996)						
HCN	95	166	Lattice	300–100	1.9×10^5	1.2×10^5
C_2N_2	35	235	ν_5	300–200	1.3×10^5	1.1×10^5
CH_3CN	95	118	Lattice	200–80	8.2×10^4	8.5×10^4
C_2H_5CN	95	221	ν_{13} or ν_{15}	250–190	1.5×10^4	8.6×10^3
C_2H_5CN	95	111	Lattice	150–80	2.4×10^4	2.1×10^4
HC_3N	95	103	Lattice	170–60	3.6×10^4	1.8×10^4

Notes. [a] This work. [b] Dello Russo & Khanna (1996, p. 380).

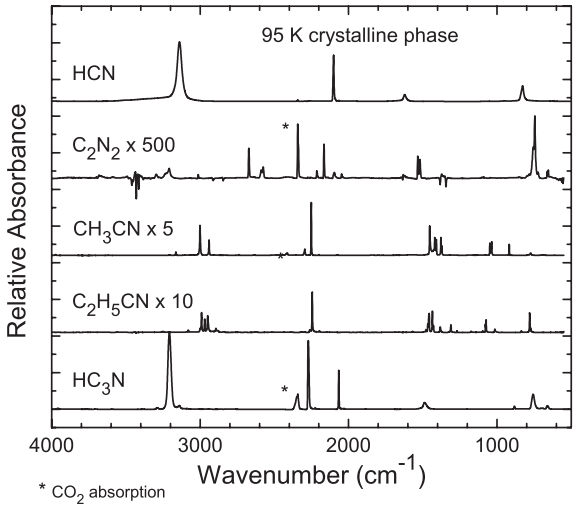

Figure 13. Infrared spectra of five crystalline nitriles, each 1 μm thick and at 95 K are compared. Spectra are stacked and scaling factors for each are shown.

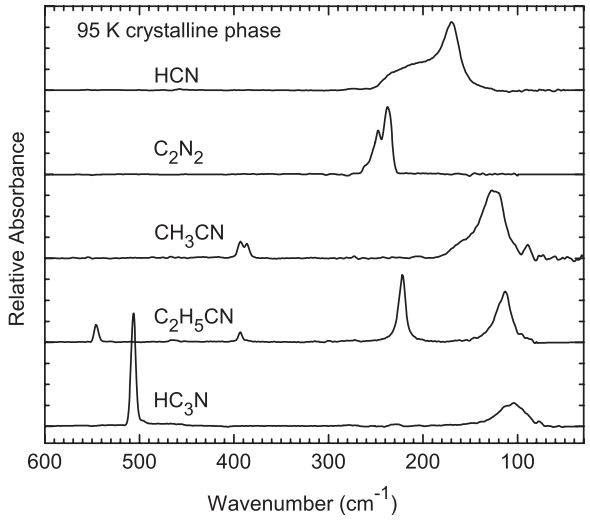

Figure 14. Absorbance spectra of five crystalline phase nitriles at 95 K are compared. Spectra are normalized to the largest absorption and are shown stacked for clarity.

Figure 14 shows the spectra of all five crystalline nitriles at 95 K, normalized to the strongest band of each molecule, from 600 to 30 cm^{-1}. Alternatively, Figure 15 is the same set of spectra plotted for a 1 μm thick ice. This plot demonstrates that C_2N_2 has the largest intrinsic band strength and that the smallest are for C_2H_5CN and CH_3CN. Table 7 compares the integrated absorbance of the strong far-infrared bands within the 300–80 cm^{-1} region with the estimated values calculated by Dello Russo & Khanna (1996).

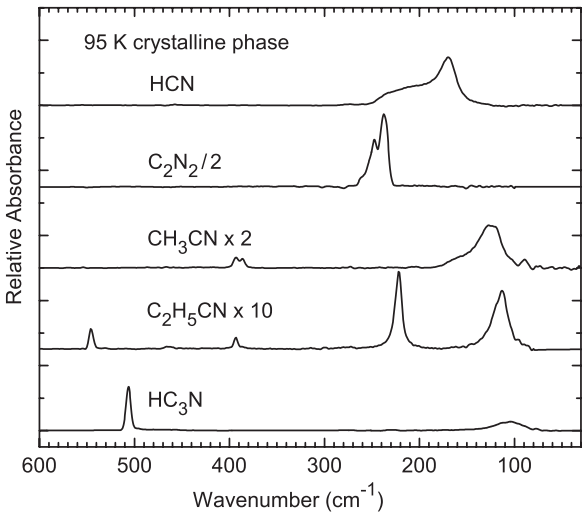

Figure 15. Absorbance spectra of 1 μm thick ices of five crystalline phase nitriles at 95 K are compared. Spectra are stacked and scaling factors for each are shown.

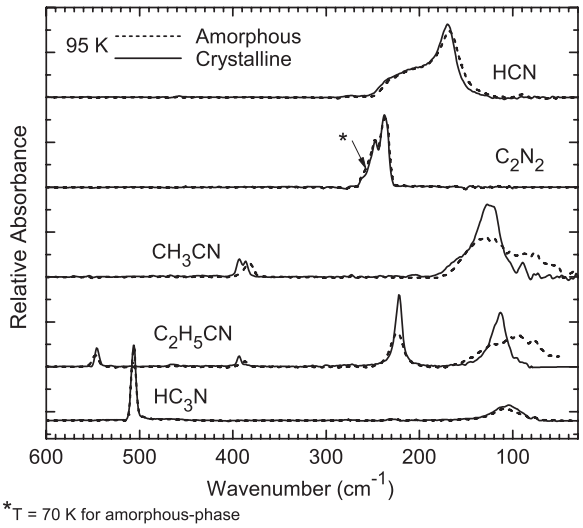

Figure 16. Absorbance spectra of five crystalline phase nitriles are compared with their amorphous phase spectra at the same temperature before annealing. Asterisk (*) means all spectra are at 95 K except for amorphous phase C_2N_2 which was at 70 K.

Figure 16 demonstrates differences in the spectra of all five nitriles in their crystalline and amorphous phases at 95 K (except for C_2N_2 which is plotted at 70 K). The broader amorphous phase bands in several cases sharpen with annealing to form the crystalline phase. Splitting occurs for CH_3CN near 400 cm^{-1}.

The extent to which the peak positions of the major crystalline-ice far-infrared bands of all five nitriles shift with

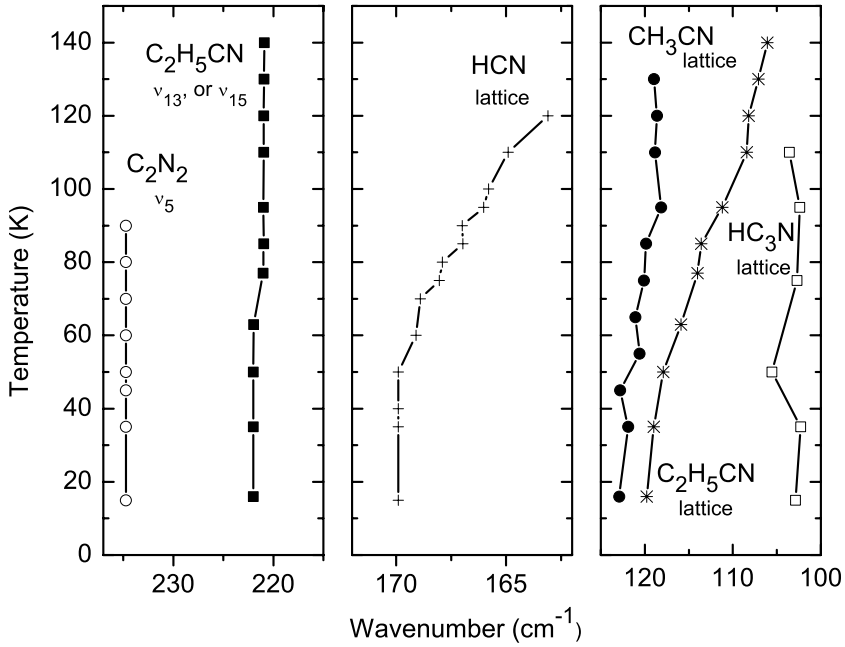

Figure 17. Temperature dependence of the position (cm^{-1}) for each of the major far-infrared absorptions in the 300–30 cm^{-1} range for five crystalline phase nitriles.

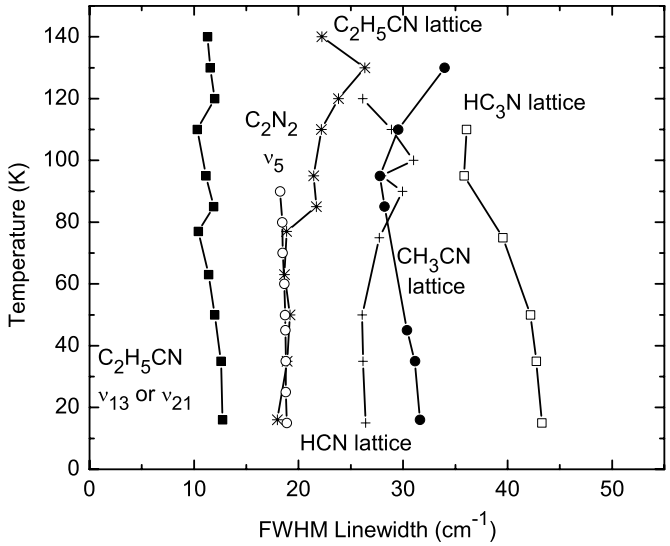

Figure 18. Temperature dependence of FWHM (cm^{-1}) for each of the major far-infrared absorptions in the 300–30 cm^{-1} region for five crystalline phase nitriles.

temperature is demonstrated in Figure 17. Here, we focus on the 240–100 cm^{-1} region and the peak positions of the major bands from each nitrile's annealing temperature down to 20 K. Plotted are the lattice bands of HCN (163.2 cm^{-1} at 120 K), CH_3CN (119.0 cm^{-1} at 130 K), C_2H_5CN (106.1 cm^{-1} at 140 K), and HC_3N (103.6 cm^{-1} at 110 K); the $\nu_5 C_2N_2$ (234.7 cm^{-1} at 90 K) and the ν_{13} or ν_{21} band of C_2H_5CN (220.9 cm^{-1} at 140 K). Because this spectral region contains observations of several unidentified broad Titan features, the implications of these thermal shifts can be considered for the relevant temperature range expected on Titan. Propionitrile has the largest band shift of ∼14 cm^{-1}; HCN has a shift of ∼7 cm^{-1}. Figure 18 demonstrates the corresponding temperature dependence of the FWHM for the same far-infrared bands.

7. CONCLUSION

For the first time mid- and far-infrared spectra and optical constants of nitrile ices known or suspected to be in Titan's atmosphere have been measured in both their amorphous and crystalline phases at a variety of temperatures. The ices were formed and annealed following published techniques and yield important information that will be of value to those who study the chemistry of Titan's atmosphere. Additionally, we provide a measured value of the 670 nm index of refraction for each amorphous and crystalline nitrile ice. All optical constants across the range of temperatures are available in digital form. Future studies will quantify differences between annealed nitrile ices and those made at high temperatures and also will provide optical constants for those samples.

The authors acknowledge support through NASA's *Cassini* Data Analysis and Planetary Atmospheres programs, and The Goddard Center for Astrobiology. We thank Mark Loeffler for measuring the index of refraction of nitrile ices at 670 nm. We acknowledge the initial driving force for new spectroscopy measurements by Raj Khanna (deceased), data sharing by Neil Dello Russo, and ongoing guidance for Titan relevance from Bob Samuelson and Carrie Anderson. We also thank an anonymous referee for helpful comments that led to the improvement of this manuscript.

REFERENCES

Anderson, C. M., Samuelson, R. E., Bjoraker, G. L., & Achterberg, R. K. 2010, Icarus, 207, 914
Berland, B. S., Brown, D. E., Tolbert, M. A., & George, S. M. 1995, J. Geophys. Res. Lett., 22, 3283
Berning, P. H. 1963, in Phys. Thin Films 1, ed. G. Haas (New York: Academic), 69
Bertie, J. E., & Zhang, S. L. 1992, Can. J. Chem., 40, 520
Bézard, G., Marten, A., & Paubert, G. 1993, BAAS, 25, 1100
Coustenis, A., Schmitt, B., Khanna, R. K., & Trotta, F. 1999, Planet. Space Sci., 47, 1305
Crowder, G. A. 1986, Spectrochim. Acta A, 42, 1229
Dello Russo, N. 1994, PhD dissertation, Univ. of Maryland

Dello Russo, N., & Khanna, R. K. 1996, Icarus, 123, 366
Dulmage, W. J., & Lipscomb, W. N. 1951, Acta Crystallogr., 4, 330
Edwards, D. F., & Philipp, H. R. 1985, in Handbook of Optical Constants of Solids: Vol. 1, ed. E. D. Palik (New York: Academic), 665
Garland, C. W., Nibler, J. W., & Shoemaker, D. P. 2002, Experiments in Physical Chemistry (New York: McGraw-Hill)
Gerakines, P. A., Moore, M. H., & Hudson, R. L. 2004, Icarus, 170, 204
Goldstein, F. 1989, in Methods of Experimental Physics, Vol. 25, ed. D. Malacara (New York: Academic), 273
Hanel, R., et al. 1981, Science, 212, 192
Harrick, N. J. 1971, Appl. Opt., 10, 2344
Hudgins, D. M., Sandford, S. A., Allamandola, L. J., & Tielens, A. G. G. M. 1993, ApJS, 86, 713
Iloukhani, H., & Almasi, M. 2009, Thermochim. Acta, 495, 139
Khanna, R. K. 2005a, Icarus, 177, 166
Khanna, R. K. 2005b, Icarus, 178, 165
Khanna, R. K., Perera-Jarmer, M. A, & Ospina, M. J. 1987, Spectrochim. Acta A, 43, 421
Kunde, V. G., Aikin, A. C., Hanel, R. A., Jennings, D. E., Maguire, W. C., & Samuelson, R. E. 1981, Nature, 191, 686
Maguire, W. C., Hanel, R. A., Jennings, D. E., Kunde, V. G., & Samuelson, R. E. 1981, Nature, 292, 683
Masterson, C. M., & Khanna, R. K. 1990, Icarus, 83, 83
Moureu, C., & Bongrad, J. C. 1920, Ann. Chim., 14, 47
Ohta, K., & Ishida, H. 1988, Appl. Spectrosc., 42, 952
Ospina, M., Zhao, G., & Khanna, R. K. 1988, Spectrochim. Acta A, 44, 23
Riddick, J. A., Bunger, W. B., & Sakano, T. K. 1986, Organic Solvents: Physical Properties and Methods of Purification (4th ed.; New York: Wiley)
Romanescu, C., Marschall, J., Kim, D., Khatiwada, A., & Kalogerakis, K. S. 2010, Icarus, 205, 695
Samuelson, R. E., & Anderson, C. M. 2009, AAS/Division for Planetary Sciences Meeting Abstracts, 41, 17.05
Samuelson, R. E., Mayo, L. A., Knuckles, M. A., & Khanna, R. J. 1997, Planet. Space Sci., 45, 941
Samuelson, R. E., Smith, M. D., Achterberg, R. K., & Pearl, J. C. 2007, Icarus, 189, 63
Sandford, S. A., & Allamandola, L. J. 1990, ApJ, 355, 357
Satorre, M. Á., Domingo, M., Millán, C., Luna, R., Vilaplana, R., & Santonja, C. 2008, Planet. Space Sci., 56, 1748
Seiber, B. A., Smith, A. M., Wood, B. E., & Muller, P. R. 1971, Appl. Opt., 10, 2086
Sill, G., Fink, U., & Ferraro, J. R. 1980, Opt. Soc. Am., 70, 724
Tempelmeyer, K. E., & Mills, D. W., Jr. 1968, J. Appl. Phys., 39, 2968
Weast, R. C. (ed.) 1986, Handbook of Chemistry and Physics (66th ed.; Boca Raton, FL: CRC Press)
Westley, M. S., Baratta, G. A., & Baragiola, R. A. 1998, J. Chem. Phys., 108, 3321
Wood, B. E., & Roux, J. A. 1982, J. Opt. Soc. Am., 72, 720